ORIGINAL ARTICLE

Accuracy of the pattern transfer from the metal mask to the workpiece surface during multiphase jet machining

Yan Hu [1] · Qingwen Dai [1] · Wei Huang [1] · Xiaolei Wang [1]

Abstract

Multiphase jet machining (MJM) is a recently developed surface texturing method based on which a mixture of abrasives and water is accelerated by compressed air to remove material from substrates. Considering the high divergence of the jet, masks are needed for MJM to obtain the desired features and dimensions. To investigate the pattern transfer accuracy, masks were prepared from a 304 stainless steel sheet using laser machining. The fundamental parameters of MJM as well as the effects of the mask opening width and thickness on the processing of the structures were studied and experimentally optimized. The use of wax to fix the mask on the substrate is proposed to avoid the frosted area around the machining structures. Overall, the optimized process MJM parameters can be used to fabricate various surface textures with the desired accuracy and dimensions.

Keywords Multiphase jet machining · Transfer accuracy · Masked surface texture

1 Introduction

The wear on mating surfaces is a serious problem, which limits the performance, stability, durability, and reliability of mechanical seals. In recent years, surface texturing has become one of the most attractive techniques used to ameliorate the tribological and sealing properties of mechanical seals [1]. Spiral grooves [2] or micro-dimples [3] on the sealing faces of dynamic and static rings effectively enhance the retention of the lubricating film and load-carrying capacity.

The high-accuracy realization of three-dimensional (3D) surface textures remains a challenge. The most common methods used to create patterned surfaces in the field of advanced manufacturing technology are laser texturing, chemical etching, and mechanical processes. Unfortunately, laser machining is easily associated with heat-affected zones as well as material pileup around the structures [4, 5]. Electrochemical machining cannot be applied to nonconductive materials such as silicon carbide [6]. Dry etching methods require expensive equipment (vacuum chambers) and are more difficult to implement [5]. Micro-cutting or milling leads to the generation of bulges or burrs, and it is hard to obtain specific shapes or dimensions [7–9].

Two-phase (air or water and abrasive) jet machining has been an effective surface texturing tool because of the low processing cost, high etching rate for a wide variety of hard-to-cut materials, good machining quality, and absence of burrs or heat-affected zones [10, 11]. Park et al. [12] used abrasive air jet machining and a driving pressure of only 0.25 MPa to fabricate grooves and holes on a glass surface. Haghbin et al. [13] and Wang et al. [14] used a driving pressure of 345 and 20–35 MPa for abrasive water jet machining, respectively. Abrasive air jet machining is more convenient and safer than abrasive water jet machining because the air-driven pressure is much lower than the water-driven one. However, abrasive air jet machining is associated with serious dust pollution.

Multiphase jet machining (MJM) based on which a mixture of abrasives and water is accelerated by compressed air to remove materials has become a new machining tool in the field of advanced manufacturing technology. This method utilizes the advantages of air jet machining under relatively low air pressure and solves problems such as abrasive recirculation and environmental pollution. The MJM was originally used for dust-free and high-performance polishing and cleaning of technical surfaces by Tsai et al. [15] and Sobczak et al. [16],

✉ Xiaolei Wang
  wxl@nuaa.edu.cn

[1] National Key Laboratory of Science and Technology on Helicopter Transmission, Nanjing University of Aeronautics and Astronautics, Nanjing 210016, China

Fig. 1 Schematic diagram of the MJM system
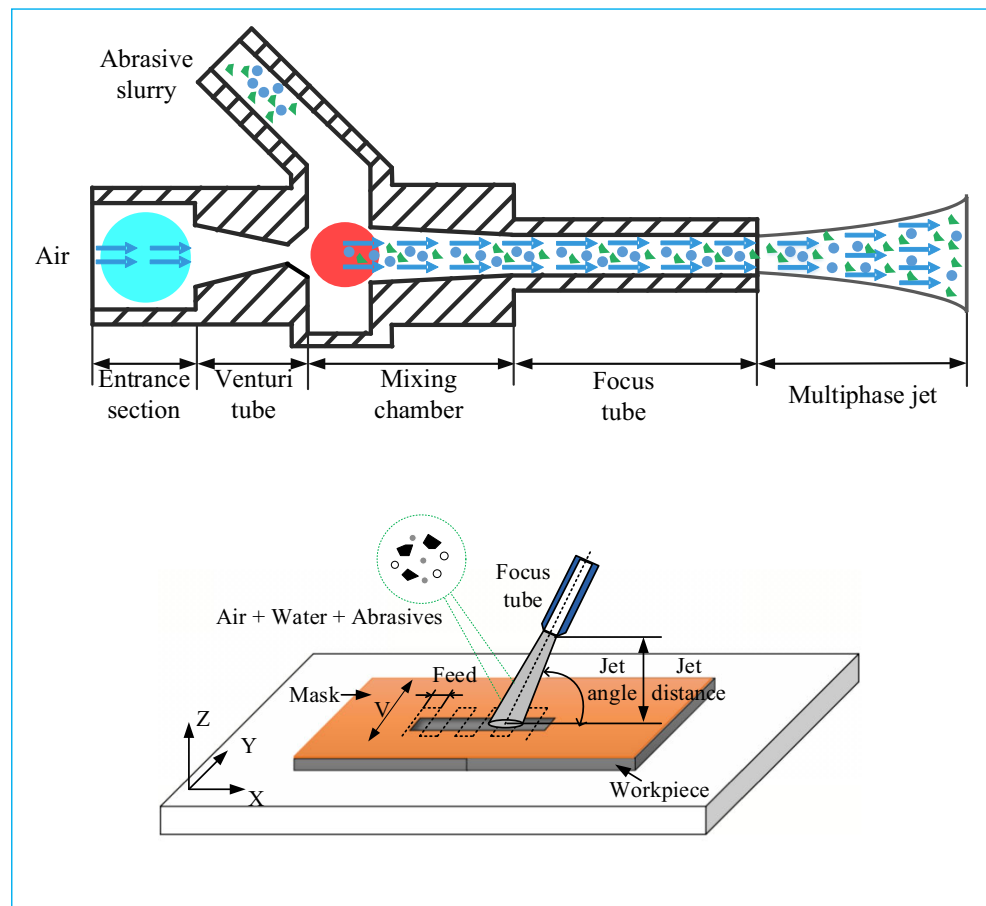
respectively. Inspired by their work, Su et al. [17, 18] used MJM for the machining of various surface textures on mating faces of mechanical seals after optimizing the nozzles and machining process.

A jet direct writing technology without masks was realized by Miller [19] who used micromachining abrasive waterjet systems with jet diameters from 30 to 70 μm. However, the air-driven jet in the MJM process is highly divergent, resulting in frosted regions at the edges of surface textures, and the air

jet footprint is several millimeters in size [20]. On the other hand, the diameter of the jet flow is not arbitrary and the jet does not have a direct writing function such as the thin waterjet. Therefore, the realization of different dimples, grooves, and other complex surface textures with various sizes using different nozzles is unlikely [21]. Erosion-resistant masks that are tightly adhered or magnetically attracted to the surface of the target material are required for MJM to obtain the desired features and dimensions, and the transfer accuracy, cost, and controllability of the mask should be taken into account [22].

Metals [18], elastomers [23], and polymers [17, 24] have been used as masking materials because of their high erosion resistance. Generally, rubber or metal plates are the main materials used for masks, which can be easily fabricated by electrochemical machining or laser cutting. Su et al. [17] and Wensink et al. [23] used copper masks fabricated by
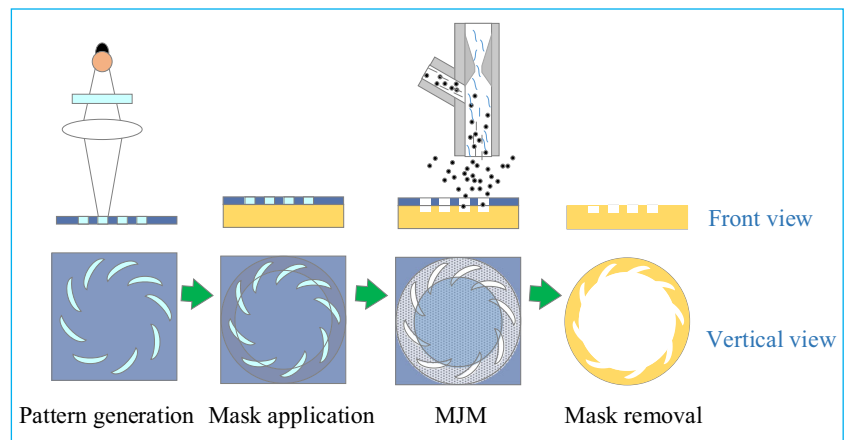
Table 1   Parameters for the MJM operating system

Venturi tube	0.7 mm
Focus tube	1.9 mm
Mask thickness	200–500 μm
Jet angle	70–90°
Air pressure	0–0.7 MPa
Jet distance	0–15 mm
Feed	50–250 μm
Nozzle motion rate	0.1–0.5 mm/s
Particle size (mesh number)	800–2000
Abrasive concentration	0–10%

Table 2   Relationship between the mesh number and particle size

Mesh number	800	1000	1200	1500	2000
Particle size, μm	18	13	10	8	6.5

Fig. 2 Steps of the MJM process

Front view

Vertical view

Pattern generation   Mask application   MJM   Mask removal

electrochemical deposition because the pattern can be easily transferred by using a photoresist template and electrolysis, but this type of mask is too thin to protect the substrate for a deeper structure and chemical post-treatment is required to remove the mask after its use. Ghobeity et al. [25] used thick steel masks instead of conventional thin, polymeric masks to improve the definition of straight channel edges on glass plates. Nouhi et al. [26] introduced an alternate shadow mask consisting of two parallel metal strips, which can be moved with the nozzle to allow direct writing during the abrasive jet micromachining, but the micro-corrosion of the boundary cannot be avoided. Belloy et al. [10] processed glass by powder blasting using 30 μm Al_2O_3 particles and obtained the maximum erosion rate at a metal mask pattern size of 500 μm. Research on metallic masks mainly focused on the fabrication of different types of resistant masks and the selection of the mask material. Few studies have been conducted to explore if the mask properties itself, such as the opening width and thickness, are related to the machining quality and cross-sectional shape of the MJM process.

Therefore, the aim of this study was the fabrication of various surface textures with desired accuracies and dimensions using MJM. Masks fabricated from a 304 stainless steel sheet using laser machining were utilized for the MJM process. The effects of the width and thickness of the mask, jet distance, jet pressure, and particle size on the frosted regions and transfer accuracy were experimentally studied. Subsequently, three typical surface textures were machined using preselected process conditions to verify the feasibility of the fabricated microstructure as mechanical seal.

2 Experiment details

2.1 Experimental setup

When compressed air passes through the nozzle at a high velocity, as shown in Fig. 1, the abrasive and water mixture is drawn into the mixing chamber based on a negative pressure created in the nozzle. Subsequently, the mixture combines with air, forming a multiphase jet, which is accelerated toward the target surface. The metal mask is fixed to the substrate using a double-sided adhesive. Based on the use of masks with certain thicknesses and wear resistances, microstructures with specific shapes and sizes can be fabricated in desired locations. The water is used for the slurry collection and transport to the machining tank such that it can be inhaled into the mixing chamber again. The surface of the workpiece is uniformly covered with abrasives and an S-type motion is used for the nozzle. The

Fig. 3 Three typical masks fabricated via laser machining. **a** Circular. **b** Rectangular. **c** Spiral
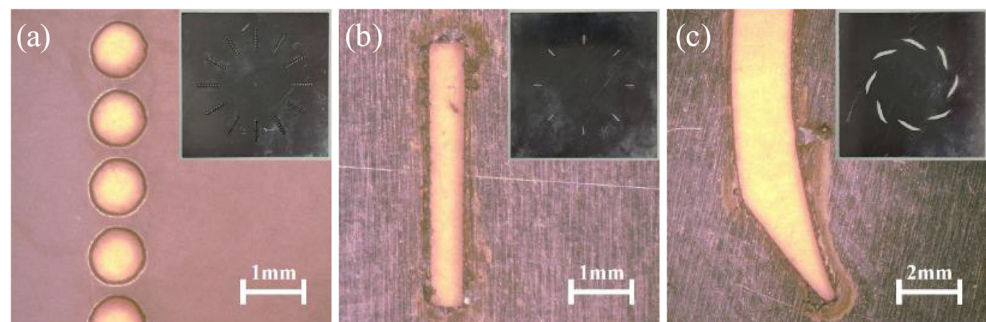
Table 3 Physical properties of SD, RBSC, and SUS304

Materials	Density; ρ, g/cm^3	Hardness	Elastic modulus; E, GPa	Tensile strength; σ_b, MPa
SD	3.52	HV 1000	1100	1050–3000
RBSC	3.05	HRA 91	330	352
SUS304	7.93	HRB 89	193	535

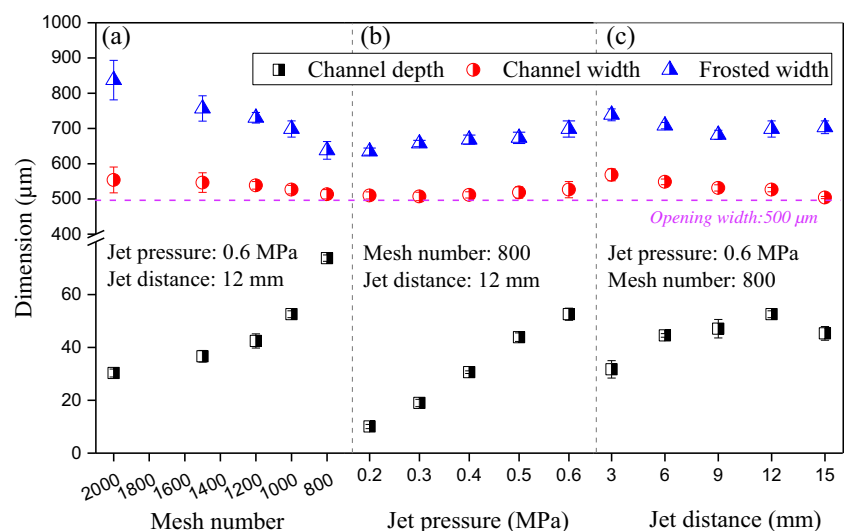parameters used for the machining process in this study are shown in Table 1.

2.2 Machining details

During the MJM process, the substrate is exposed to a slurry-laden air jet with a pressure ranging from 0.2 to 0.6 MPa and diamond abrasive particles with mesh numbers ranging between 800 and 2000. The relationship between the mesh number and particle diameter is shown in Table 2. All process steps are summarized in Fig. 2. As a typical hard and brittle material, a reaction-bonded silicon carbide (RBSC) ring was used as mechanical seals for the machining test. To machine microstructures with proper morphologies and dimensions in desired locations, SUS304 was selected as mask material in this study because of its good erosion resistance and machining properties. Figure 3 shows three typical masks with circular, rectangular, and spiral shapes, respectively, that were fabricated from a 304 stainless steel sheet (200 μm thick) using laser machining.

The main material properties of RBSC, synthetic diamond (SD), and SUS304 are listed in Table 3. The structures were analyzed after the process using a digital microscope (KEYENCE, Japan) and 3D optical profilometer (Bruker, USA).

SD synthetic diamond, *RBSC* reaction-bonded silicon carbide

3 Results and discussion

3.1 Effects of fundamental MJM parameters

To obtain the desired pattern transfer accuracy and high machining efficiency, the fundamental MJM parameters, including the particle mesh number, jet pressure and jet distance, were firstly optimized using experiments. The frosted width is defined as the rough corrosion zone caused by particles entering the voids between the mask and substrate.

Figure 4 illustrates the effects of the particle mesh number, jet pressure, and jet distance on the machining. As shown in Fig. 4a, the particle mesh number significantly affects the machining. A smaller mesh number yields a deeper channel depth and thus improves the machining efficiency, which is mainly due to the fact that the kinetic energy of the impact of large particles is higher than that of small particles. The channel width decreases with decreasing mesh number. It has been reported that, in contrast to larger particles, smaller particles can pass through narrower openings without impinging on the mask, resulting in narrower channels in a larger-particle erosion environment [27]. It is easier for smaller particles to enter the voids, leading to wider frosted zones. Consequently, a mesh number of 800 should be chosen for the MJM process. Figure 4b, c shows that the jet pressure and jet distance have inconspicuous effects on the widths of the frosted zones and channels.

Fig. 4 Channel depth, channel width, and frosted width depending on various parameters used for MJM under identical experiment conditions (abrasive concentration of 10%, jet angle of 90°, feed of 100 μm, and nozzle motion rate of 0.2 mm/s)
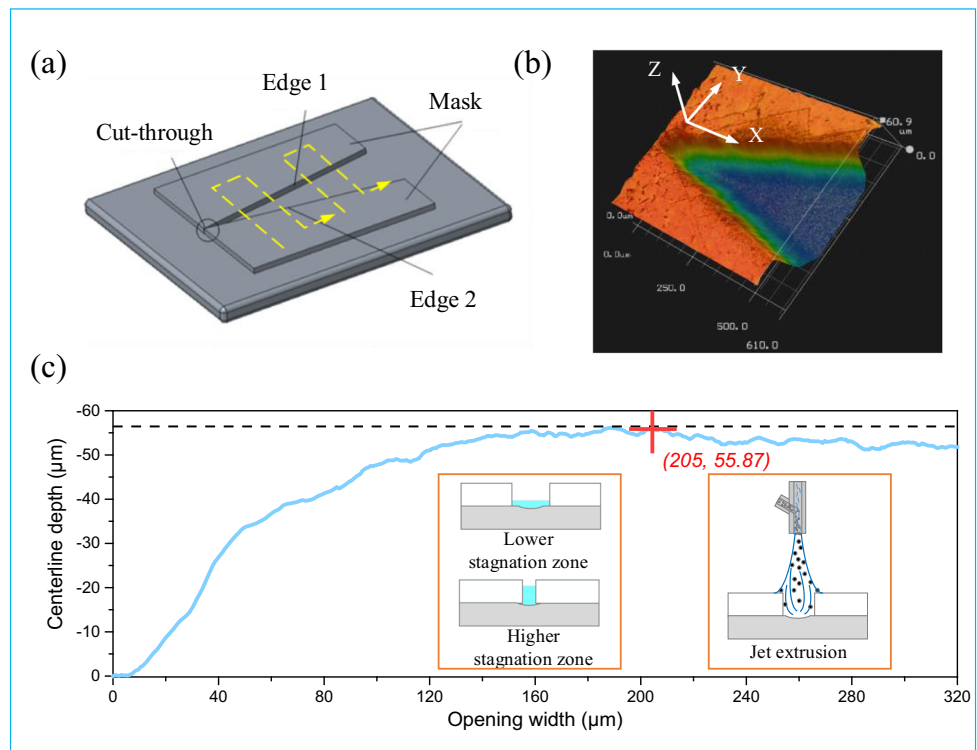
Fig. 5 **a** V-shape of the mask, **b** 3D morphologies of the channel after processing, and **c** channel centerline depth depending on the opening width

To achieve a higher machining efficiency, a jet distance of 12 mm and jet pressure of 0.6 MPa should be preferred. With these optimized fundamental parameters, the effects of the mask-geometry on the machining were investigated in the following sections.

3.2 Effects of the mask-geometry

3.2.1 Effect of the mask opening width, *w*

Due to the variations in the slurry flow flux, the mask opening size may affect the machining efficiency and cross-sectional profile. As shown in Fig. 5a, a V-shaped mask opening with a thickness of 200 μm and a width ranging from 0 to 320 μm was designed to evaluate the processing ability of MJM. The whole surface was exposed to a uniform particle flux using an S-type feed mode, 10% mass concentration of SD, jet pressure of 0.6 MPa, jet distance of 12 mm, jet angle of 90°, feed of 150 μm, nozzle motion rate of 0.2 mm/s, and mesh number of 800. The processing results are shown in Fig. 5b, c.

Figure 5c shows the change of the channel centerline depth depending on different mask opening widths, indicating that the opening width notably affects the depth. The depth curve can be divided into three regions. When the opening size is smaller than 140 μm, the channel depth notably decreases. The etching depth at *w* = 20 μm is only 8% of the depth at *w* = 140 μm. The maximum channel depth is obtained in the

width range of 140–220 μm. Beyond an opening width of 220 μm, the etching depth slightly decreases and eventually reaches a relatively steady state.

Figure 6 shows the surface topography of the processed workpiece, indicating different characteristics on both sides of the channel. The narrow opening is almost free of frosted zones, but notable frosted area (called overexposure area) can be observed (red dashed circle) at an opening width of 200 μm. At a larger opening width, only a slight symmetrical frosted area is observed on both sides of the channel. As
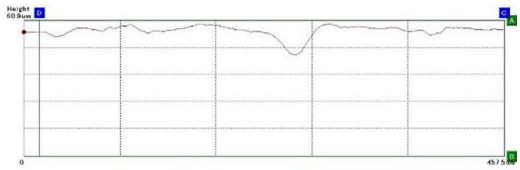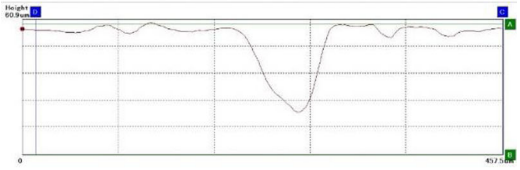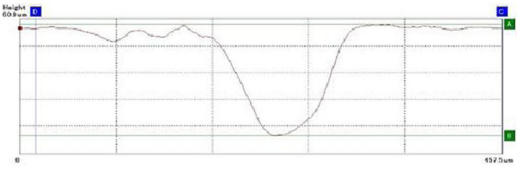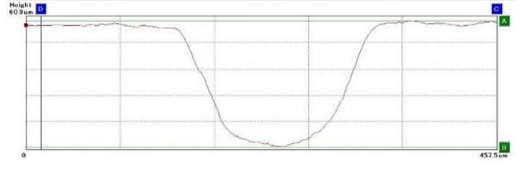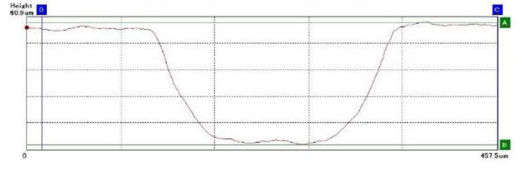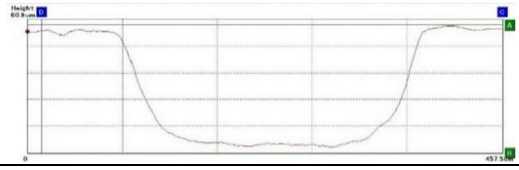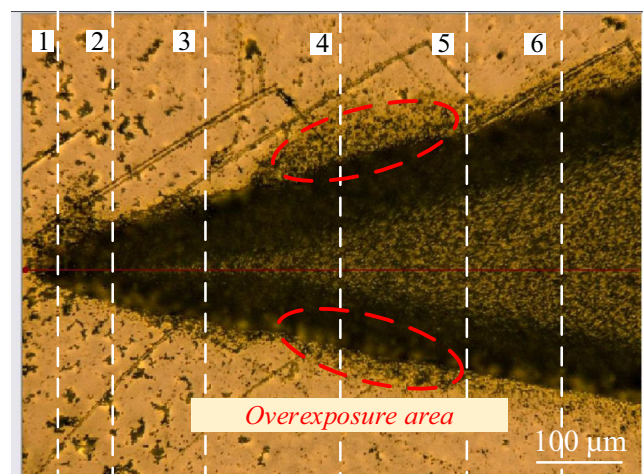

Fig. 6 Surface topography of the processed workpiece and positions on the top of the channel for the shapes of Y cross section

Table 4 Channel shapes of the Y cross section at the positions shown in Fig. 6

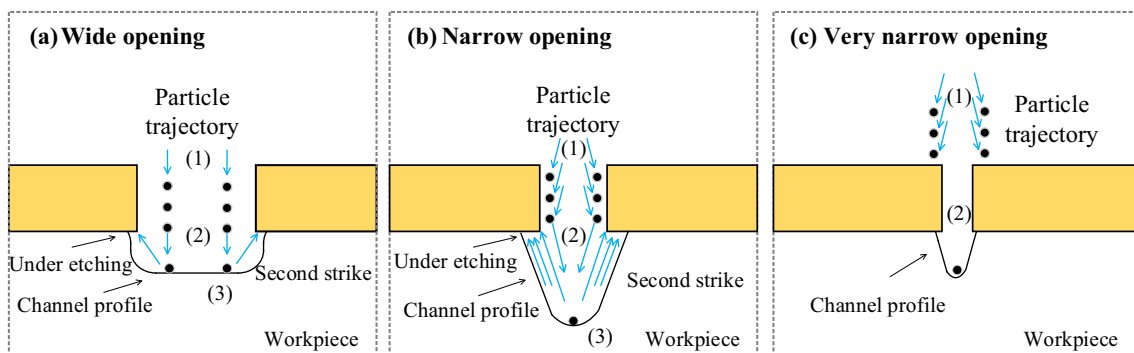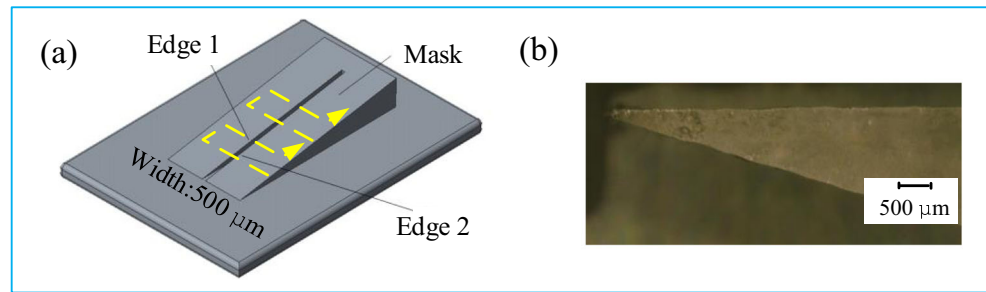| Position	Channel width, μm	Opening width, μm	Shape of the Y cross section
1	50	35	
2	100	78	
3	150	118	
4	200	171	
5	250	232	
6	300	286	

Fig. 7 Schematic of the secondary impact and sidewall reflection of particles for a **a** wide mask, **b** narrow mask, and **c** very narrow mask

shown in Table 4, the shape of the Y cross section changes from V- to U-shape with a relatively smooth bottom when the opening width increases from 50 to 300 μm. When the opening width is smaller than 200 μm, the channels are V-shaped. When the opening width is greater than 200 μm, the channels are U-shaped. The channel shape changes in the overexposed area, which is unexpected. The channel width is wider than the opening width of the mask, especially in the overexposed area.

Because the multiphase jet is highly divergent, the sweeping of the jet over the mask leads to unavoidable phenomena including particle wall and bottom reflections. The particle wall reflections are also called "blast lag" effect based on which a narrower channel more quickly develops an inclined sidewall and forms a V-shaped profile at the center of the particle intersection [28]. As described in more detail by Wensink and Elwenspek [28], a narrower mask opening leads to the quick generation of a V-shaped channel because of the blast lag. Based on air-driven AJM of masked channels [10, 26, 28], it is known that such secondary particle reflections cause a significant increase in the centerline erosion rate and channel width. Considering that these studies are fragmented, a systematic and auxiliary explanation of the effect of the opening width on machining is required.

Figure 7a shows that a U-shaped channel with a flat bottom is generated by the impact of uniform particles when the opening is relatively wider. Particle bottom reflections lead to the generation of small frosted areas on both sides of the channel and the channel width is slightly larger (by 5–7%) than the

opening width. Figure 7b shows that the opening width decreases due to the increase in the particle wall and bottom reflections, producing a larger frosted area (overexposure area) near the edges of the surface texture. Because narrow opening sidewalls lead to the reflection of the particles to the channel centerline, a V-shaped channel with a deeper centerline forms in the overexposure area. The particle bottom reflections notably increase the widths of the channel and frosted zone in the overexposure area. Figure 7c shows that it is hard for the abrasive particles to enter the opening and erode the channel when the opening width is too narrow, leading to a decrease in the processing efficiency. Apart from the effect of the narrower opening width, one difference between dry air abrasive jet (AAJ) machining and MJM is that the abrasive slurry used in this technology has a larger stagnation zone in the narrower channel according to Matsumura's research [29], leading to the reduction in the etching rate of narrower channels.

3.2.2 Effect of the mask thickness, t

Because of the reflection of the particles on the side of the mask opening, the mask thickness also affects the machining efficiency and erosion profile. To study the effect of the mask thickness, a wedge mask with an opening of 500 μm was designed shown in Fig. 8a, b. The thickness of the mask ranges from 0 to 8 mm. The experimental conditions used in this section are the same as those described above.

Fig. 9 Widths of the frosted area (a) and channel (b), which decrease with increasing mask thickness
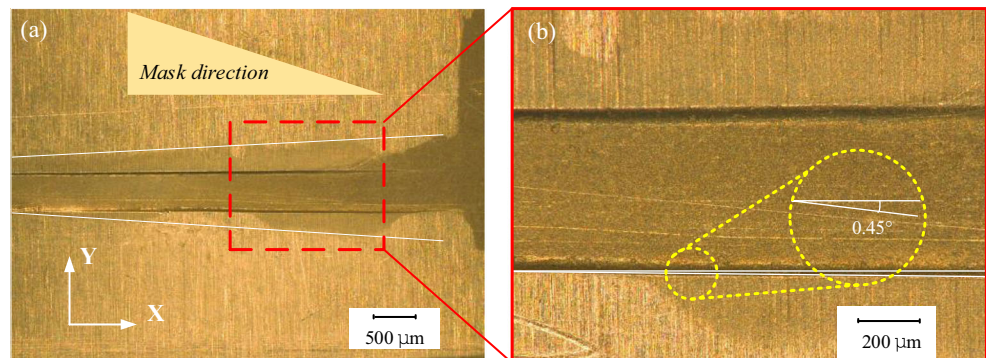
Fig. 10 Channel depth (**a**) and shape (**b**) depending on the mask thickness
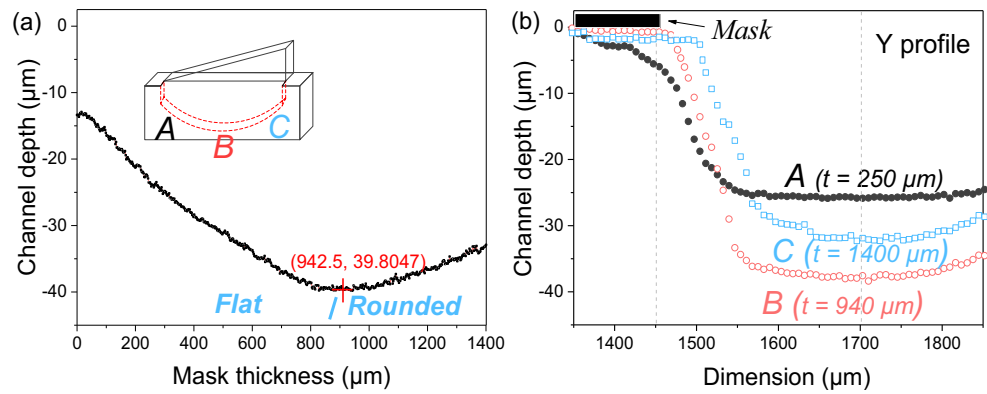

Figure 9a shows the topography of the machined workpiece. The rough areas (frosted areas) on both sides of the channel are marked by white lines. The frosted areas are wider and narrower at locations at which the mask is thinner and thicker, respectively. The enlargement of the red inset in Fig. 9b illustrates that the width of the channel is slightly wider than that of the opening of the thin mask because of particle bottom reflections. For example, the channel width at a mask thickness of 300 μm is 1.4 times the width of the opening. However, the channel width is slightly narrower than the opening width when the mask is thicker, which indicates that the channel edges can be brought closer to the mask opening when a suitable thickness (from 800 to 1000 μm) is used. Figure 10a shows the channel centerline depths at different mask thicknesses, indicating that the mask thickness notably affects the channel depth. The maximum channel depth is achieved when the mask thickness is ~900 μm, indicating that both too thick and too thin masks lead to a decrease in the machining efficiency. Figure 10b shows the three typical channel shapes at the A ($t = 250$ μm), B ($t = 940$ μm), and C ($t = 1400$ μm) positions marked in Fig. 10a, indicating that the bottom of the channel changes from flat to rounded with increasing mask thickness.

These changes can also be attributed to the variations in the slurry flow rate due to differences in the particle reflection at the border of the opening. The increase in the channel and frosted widths in thinner masks can partly be attributed to the secondary slurry flow along the channel length but is mostly due to the fact that a thinner opening allows more abrasive particles to reach the voids with sufficient kinetic energy to cause boundary erosion. The machining efficiency of the thin mask is lower because the slurry flow spreads into all directions. With increasing mask thickness, masks with medium thickness lead to the reflection of the particles to the channel centerline and thus to an increase in the machining efficiency and the change of the channel profile (from U- to V-shaped). At a higher thickness, the particles impacting the opening edge are more likely to bounce back onto the relative edge. The erosion rate of a thicker opening decreases due to the larger sidewall reflection of particles and the transfer of less kinetic energy to the target surface.

4 Reduction of the width of the frosted zone

Because a plate is never completely flat, there are voids between the mask and substrate, leading to the formation of frosted zones by particles entering the voids, as shown in

Fig. 11 Schematic showing **a** how the mask clamped or pasted onto the substrate produces a gap and frosted area and **b** how the protection layer (wax seal) prevents the entering of the particles
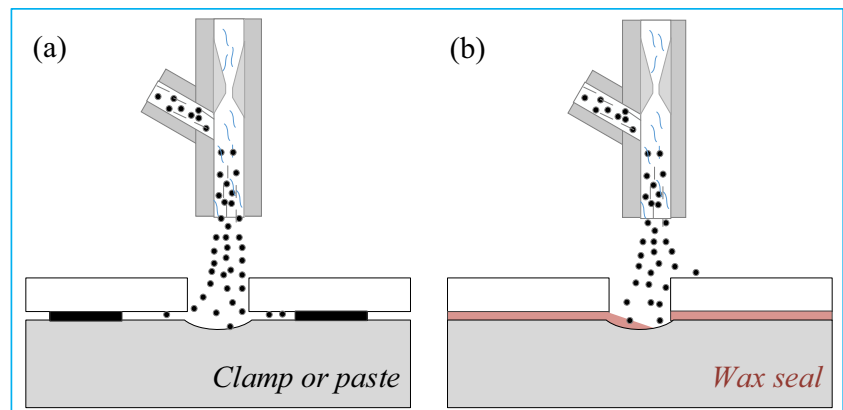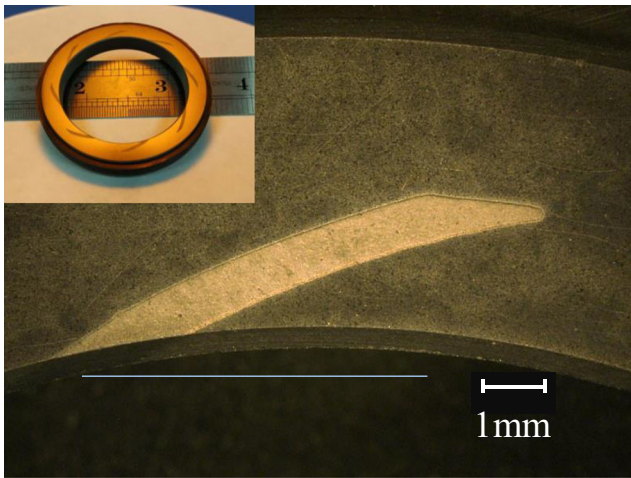
Fig. 12 Spiral channels with wax seal for upstream pumping seal machined using MJM (12 mm jet distance, 0.6 MPa jet pressure, 10% mass concentration, 90° jet angle, feed of 100 μm, nozzle motion rate of 0.2 mm/s, and mesh number of 800)

Fig. 11a. To prevent this, wax (W100, 50–60 °C softening point) can be used. Wax is a brittle material and good adhesive after melting and meets the requirements of an intermediate protection or adhesion layer shown in Fig. 11b. In this study, wax was spread on the heated mask at 70 °C. Subsequently, the substrate was added to the mask and the mask was cooled to room temperature. The wax acts as binder instead of glue (double adhesive) between the substrate and mask and forms a very tight and strong connection. It can prevent particles from entering the gap and causing corrosion. The positive effect of the intermediate layer is shown in Fig. 12 (after machining), indicating that the spiral channels of the upstream pumping seal have a good processing quality and boundary.

Figure 13 shows the partial 3D profiles of the three typical surface textures machined using MJM (12 mm jet distance, 0.6 MPa jet pressure, 10% mass concentration, 90° jet angle, 0.2 mm/s nozzle motion rate, 800 mesh number, and 800 μm mask thickness). For the machining of all channels, wax was applied between the mask and substrate during the machining process. Figure 13 shows the photos of a channel at 50 μm feed with a width and average depth of ~500 and 106.5 μm,

respectively (Fig. 13a); dimple at 50 μm feed with a diameter and average depth of ~1 mm and 87.6 μm, respectively (Fig. 13b); and spiral groove at 100 μm feed with an average depth of ~15 μm (Fig. 13c). These machined features confirm that the MJM process has a great potential for machining surface textures of mechanical seals with complex patterns on the mating surfaces.

5 Conclusions

In summary, MJM is an effective and cheap directional etching technique for brittle materials, which can be used to machine surface textures of mechanical seals that are impossible or difficult to machine using traditional tools. The following conclusions can be drawn:

1. The use of particles with a mesh number of 800 is preferred for the MJM process to achieve a higher machining efficiency, create a channel edge close to the mask, and reduce the width of the frosted area.
2. With respect to the opening width, the channel depth notably decreases when the opening width is less than 140 μm. The maximum channel depth is achieved in the width range of 140–220 μm. Beyond an opening width of 220 μm, the etching depth slightly decreases and eventually reaches a relatively steady state. At the opening width of 200 μm, the channel shape changes from V- to U-shaped.
3. With respect to the mask thickness, the maximum channel depth and a relative flat bottom surface can be achieved with a mask thickness of 900 μm. A decrease or increase of this mask thickness leads to the decrease in the machining efficiency.
4. The use of a wax seal leads to a significant reduction of the frosted area in the MJM process. Based on the use of optimized machining parameters, MJM has a great potential for the effective and economic machining of microstructures on surfaces of mechanical seals.
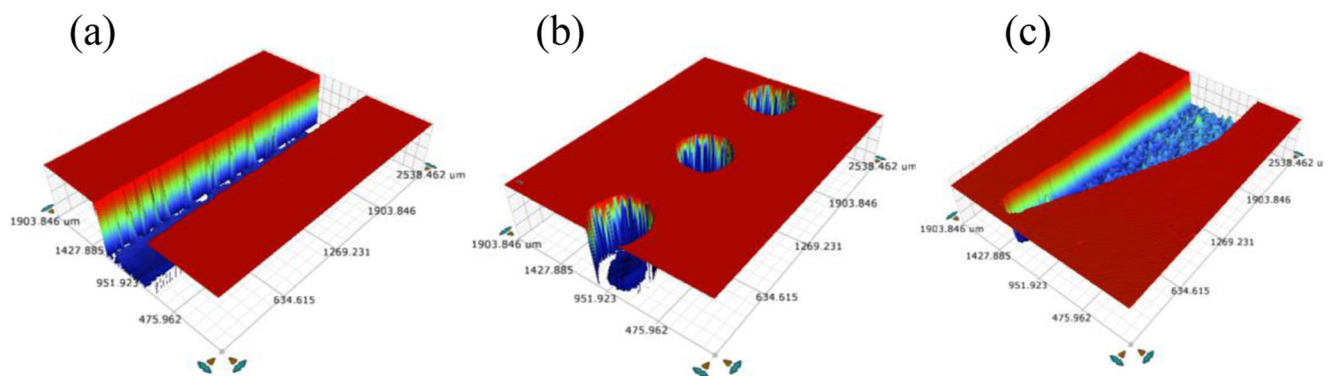

Fig. 13 Partial 3D profile of the three typical surface textures machined using MJM. **a** Channel. **b** Dimples. **c** Spiral groove

References

1. Wang XL, Adachi K, Otsuka K, Kato K (2006) Optimization of the surface texture for silicon carbide sliding in water. Appl Surf Sci 253(3):1282–1286

2. Shi LP, Wang XY, Su X, Wei H, Wang XL (2015) Comparison of the performances of mechanical gas seals textured with micro-grooves and micro-dimples. J Tribol 138(2):88–90

3. Wang XY, Shi LP, Dai QW, Huang W, Wang XL (2018) Multi-objective optimization on dimple shapes for gas face seals. Tribol Int 123:216–223

4. Etsion I (2005) State of the art in laser surface texturing. Trans ASME J Tribol 127(1):761–762

5. Coblas DG, Fatu A, Maoui A, Hajjam M (2015) Manufacturing textured surfaces: State of art and recent developments. Proc IME J J Eng Tribol 229(1):3–29

6. Qian SQ, Zhu D, Qu NS, Li HS, Yan DS (2010) Generating micro-dimples array on the hard chrome-coated surface by modified through mask electrochemical micromachining. Int J Adv Manuf Technol 47(9-12):1121–1127

7. Wu X, Li L, He N (2017) Investigation on the burr formation mechanism in micro cutting. Precis Eng 47:191–196

8. Chae J, Park SS, Freiheit T (2006) Investigation of micro-cutting operations. Int J Mach Tool Manu 46(3):313–332

9. Zhang T, Liu ZQ, Xu CH (2013) Influence of size effect on burr formation in micro cutting. Int J Adv Manuf Technol 68(9-12):1911–1917

10. Belloy E, Thurre S, Walckiers E, Sayah A, Gijs MAM (2000) The introduction of powder blasting for sensor and microsystem applications. Sensors Actuators A Phys 84(3):330–337

11. Haghbin N, Spelt JK, Papini M (2015) Abrasive waterjet micro-machining of channels in metals: comparison between machining in air and submerged in water. Int J Mach Tool Manu 88:108–117

12. Park DS, Cho MW, Lee H, Cho WS (2004) Micro-grooving of glass using micro-abrasive jet machining. J Mater Process Technol 146(2):234–240

13. Haghbin N, Ahmadzadeh F, Papini M (2018) Masked micro-channel machining in aluminum alloy and borosilicate glass using abrasive water jet micro-machining. J Manuf Process 35:307–316

14. Wang FC, Xu QW, Feng DC, Guo CW (2017) Experiment study on performance of abrasive slurry jet with or without high polymer in stainless steel machining. Int J Adv Manuf Technol 95(1):1–8

15. Tsai FC, Yan BH, Kuan CY, Huang FY (2008) A Taguchi and experimental investigation into the optimal processing conditions for the abrasive jet polishing of SKD61 mold steel. Int J Mach Tool Manu 48(7):932–945

16. Sobczak R, Prazmo J, Perec A, Chmielik I (2016) Dust free surface treatment parameters of the three-phase jet, generated in the sandbot device. MM Sci J 01:872–876

17. Su X, Shi LP, Huang W, Wang XL (2016) A multi-phase micro-abrasive jet machining technique for the surface texturing of mechanical seals. Int J Adv Manuf Technol 86(5-8):1–8

18. Shi LP, Fang Y, Dai QW, Huang W, Wang XL (2017) Surface texturing on SiC by multiphase jet machining with microdiamond abrasives. Mater Manuf Process 33(13):1415–1421

19. Miller DS (2004) Micromachining with abrasive waterjets. J Mater Process Technol 149(1):37–42

20. Papini M, Ciampini D, Krajac T, Spelt JK (2003) Computer modelling of interference effects in erosion testing: effect of plume shape. Wear 255(1):85–97

21. Haghbin N, Ahmadzadeh F, Spelt JK, Papini M (2016) High pressure abrasive slurry jet micro-machining using slurry entrainment. Int J Adv Manuf Technol 84(5-8):1031–1043

22. Zhang L, Kuriyagawa T, Yasutomi U, Zhao J (2005) Investigation into micro abrasive intermittent jet machining. Int J Mach Tool Manu 45(7-8):873–879

23. Wensink H, Jansen HV, Berenschot JW, Elwenspoek MC (2000) Mask materials for powder blasting. J Micromech Microeng 10(2):175–180

24. Saragih AS, Ko TJ (2009) A thick SU-8 mask for microabrasive jet machining on glass. Int J Adv Manuf Technol 41(7-8):734–740

25. Ghobeity A, Krajac T, Burzynski T, Papini M, Spelt JK (2008) Surface evolution models in abrasive jet micromachining. Wear 264(3):185–198

26. Nouhi A, Lari MRS, Spelt JK, Papini M (2015) Implementation of a shadow mask for direct writing in abrasive jet micro-machining. J Mater Process Technol 223:232–239

27. Ghobeity A, Papini M, Spelt JK (2009) An analytical model of the effect of particle size distribution on the surface profile evolution in abrasive jet micromachining. J Mater Process Technol 209(20):6067–6077

28. Wensink H, Elwenspoek MC (2002) Reduction of sidewall inclination and blast lag of powder blasted channels. Sensors and Actuators a-Physical 102(1-2):157–164

29. Matsumura T, Muramatsu T, Fueki S (2011) Abrasive water jet machining of glass with stagnation effect. CIRP Ann Manuf Technol 60(1):355–358